

On universality and non-universality for a quantum dot in the Kondo regime

A. F. Izmaylov¹, A. Goker², P. Nordlander² and B. A. Friedman³

¹ Department of Chemistry

² Department of Physics and Department of Electrical and Computer Engineering

Rice Quantum Institute

Rice University

Houston, TX 77251-1892, USA

³ Department of Physics

Sam Houston State University

Huntsville, Texas 77341, USA

E-mail: nordland@rice.edu

Abstract. The time-dependent non-crossing approximation is employed for the single-electron transistor to calculate the transient response of the conductance for a variety of temperatures and biases. We consider the case when the dot-lead tunneling constant is suddenly changed such that the Kondo effect is present in the final state. In the fast non-universal timescale, which was previously identified [1, 2], we see rapid oscillations. The frequency of these oscillations is equal to the dot level and their amplitude is modulated by the initial and final tunneling constants. To study the slow universal timescale, we develop a new numerical scheme. We compute the conductance for two systems which have different Kondo temperatures down to a fraction of T_K in infinitesimal bias with this scheme. We conclude that universality is preserved as a function of T/T_K . We also investigate the decay rate of recently identified SKP oscillations down to zero temperature and compare it with the previous analytical results obtained with the perturbative renormalization group.

PACS numbers: 72.15.Qm, 85.30.Vw, 73.50.Mx

1. Introduction

In comparison to equilibrium conditions, there exists a poor understanding of the nonequilibrium real-time evolution of quantum many body systems. Nonequilibrium effects are quite important to understand dissipation and decoherence in electron transport through nanodevices. Quantum dots and qubits fall into this category where a mesoscopic device interacts with a fermionic or bosonic bath. Advances in the construction of quantum dots have made it possible to study in a controlled fashion nonequilibrium phenomena even though most experiments have been limited to steady state transport. However, recently Elzerman *et al.* have emphasized practical importance of real-time dynamics in quantum dots for quantum computation[3]. This type of system constitutes an ideal platform to study the Kondo effect out of equilibrium, since one can electrically tune the parameters of quantum dots. The Kondo effect was first discovered in bulk metals with magnetic impurities providing localized unpaired spins [4] and observed later in semiconductor quantum dots [10, 11, 12]. It is an intricate many-body effect in which conduction electrons in the vicinity of a spin impurity screen the spin to form a collective entangled ground state at low temperatures[5]. The most evident connection between Kondo physics and quantum dots is when an odd number of electrons are confined within the dot. The resulting net spin is coupled to the fermionic bath at low temperatures and a sharp peak forms at the Fermi level in the dot density of states. The manifestation of this Kondo peak in physical observables is a large enhancement of the dot's conductance, which is strongly dependent on temperature, bias, and magnetic field.

Theoretical predictions [7, 8, 9] of the signature of the Kondo effect in quantum dots for steady state conduction began almost two decades ago. The anticipation that the time dependent experiments are not far behind, has recently spurred a number of theoretical groups [13, 14, 15, 17, 18, 19] to consider the effects expected when sinusoidal biases or gate potentials are applied. Indeed recent experiments[20] have now seen Kondo sidebands. In addition, the predictions [21] of split Kondo conductance peaks have been observed in double [22] and multiple [23] dots. However, the application of steps or pulses, which can provide a less ambiguous measure of timescales than ac modulation, has received much less attention theoretically [17, 24, 25, 6]. When a step is applied to the system which increases the coupling between the leads and the dot such that the system is shifted into the Kondo regime, the conductance of the dot starts to increase. The current saturates when the system reaches its new steady state configuration. In this paper, we calculate the time-dependent conductance by using the non-crossing approximation(NCA) after the coupling constant is switched to its final value, for a variety of temperatures.

Recent approaches that are complementary to the time dependent NCA used here include the determination of exact spin correlation functions at the Toulouse point [16], the dynamical $1/N$ approach to time-dependent currents through the dot [6] and time dependent numerical renormalization-group [2]. The last approach looks particularly

promising since it does not rely on any approximation and it seems to give reliable results both at temperatures much smaller than T_K and in finite magnetic fields.

2. Method

The quantum dot is modeled by a single spin degenerate level of energy ε_{dot} coupled to leads through tunnel barriers. This system is described by the Anderson Hamiltonian given by

$$H(t) = \sum_{\sigma} \varepsilon_{\sigma}(t) n_{\sigma} + \sum_{k\sigma} \varepsilon_k n_{k\sigma} + \frac{1}{2} \sum_{\sigma} U_{\sigma,\sigma'} n_{\sigma} n_{\sigma'} + \sum_{\sigma k} [V_k(t) c_{k\sigma}^{\dagger} c_{\sigma} + \text{H.c.}], \quad (1)$$

where c_{σ}^{\dagger} creates an electron of spin σ in dot level, with n_{σ} the corresponding number operator; $c_{k\sigma}^{\dagger}$ creates an electron in the leads. The Coulomb repulsion energy is given by U , which we assume to be infinitely large, preventing the dot from being doubly occupied.

For infinitesimal bias across the dot, the general features of the static spectral density when the dot level ε_{dot} is sufficiently below the Fermi level are well known. There is a broad resonance of half-width

$$\Gamma(\varepsilon_{dot}, t) = 2\pi \sum_k |V_k(t)|^2 \delta(\varepsilon_{dot} - \varepsilon_k) \quad (2)$$

around the dot level. This is inhomogeneous broadening due to the tunneling of electrons between the dot and the leads and is sometimes referred to as the Fano resonance.

In addition to the Fano resonance, there is a sharp temperature sensitive resonance at the Fermi level (the Kondo peak), characterized by the low energy scale T_K (the Kondo temperature),

$$T_K = D \left(\frac{\Gamma}{4D} \right)^{\frac{1}{2}} \exp \left(-\frac{\pi |\varepsilon_{dot}|}{\Gamma} \right), \quad (3)$$

where D is a high energy cutoff equal to half bandwidth when modeled by a symmetric flat band. Our calculations here use a symmetric parabolic band of half bandwidth $D_0 = 9\Gamma$ and $D \simeq D_0/\sqrt{e}$, the choice that gives the correct normalization for the leading logarithmic corrections in the Kondo model[29].

We use the non-crossing approximation (NCA), which is reliable for temperatures down to $T < T_K$ [27]. The details of the time-dependent method of solution have been described in previous publications[30, 29]. In this paper, we use atomic units with $\hbar = k_B = e = 1$. In the regions of parameter space where T_K , T , and V are much smaller than ε_{dot} and Γ , physical observables are functions of T/T_K , V/T_K and $T_K t$ alone, if the quantity under consideration is made dimensionless by appropriate factors of T_K and $G_0 \equiv 2(e^2/2\pi\hbar)$. We will be investigating the properties in this universal region in the second half of this paper.

We compute the electric currents through a dot which has left-right symmetry. The current into the dot depends on the time t as

$$I_{\text{in}}(t) = i \sum_{k\sigma} V_k(t) \langle c_{k\sigma}^\dagger(t) c_\sigma(t) \rangle + \text{c.c.} \quad (4)$$

It can be divided into contributions $I_{\text{left}}(t)$ and $I_{\text{right}}(t)$ by restricting the k summations to the appropriate lead. The transport current is given by $I(t) = \frac{1}{2}[I_{\text{left}}(t) - I_{\text{right}}(t)]$, which is obtained by calculating the Keldysh propagators corresponding to the angular-bracketed expectation values in Eq. (4) for each lead.

Two timescales have been identified for the application of a step or pulse[1, 2]. The first timescale corresponds to the charge relaxation and it is associated with the reshaping of the lifetime broadening of dot. This is the non-universal non-Kondo timescale and it is inversely proportional to Γ . The second timescale is related to the spin relaxation that gives rise to the formation of the sharp Kondo resonance. It is the universal Kondo timescale and it is inversely proportional to T_K . In this paper, we are largely motivated with these observations and analyze the conductance in the non-universal and universal timescales. In the non-universal timescale, we observe fast oscillations. Since this timescale corresponds to the charge relaxation, we provide a qualitative explanation to these oscillations by solving the Anderson Hamiltonian for $U=0$. In the universal timescale where Kondo resonance formation takes place, we compare the conductance results of two systems which have different Kondo temperatures. These two systems have a constant dot level and their dot-lead tunneling constant is abruptly switched at $t = t_1$ from a value, for which the current at the applied bias is small, and $T_K \ll T$, to a value for which the Kondo effect will be present. In fact, this amounts to abruptly changing the hopping term in the Hamiltonian as it can be clearly seen from Eq. (2).

Our studies all start from steady state at $t = t_0$ with bias V across the dot, where the tunneling constant Γ_1 is at a value such that the initial Kondo temperature is much smaller than the physical temperature T , and the initial conductance is so small as to be negligible. In practice, we start with $\epsilon_{\text{dot}} = -5\Gamma_1$ for time $t < t_1$. At $t = t_1$ we suddenly change the tunneling constant from Γ_1 to Γ_2 , with ϵ_{dot} unchanged. We carry out calculations for two systems and refer to them as *system one* and *system two*. They have $T_K=6.38$ K and $T_K=3.19$ K respectively.

In order to tackle the two timescales in this problem, we absorbed the oscillation frequencies of retarded and less than Green's functions into the kernel in the Dyson equations and thus obtained smooth Green's functions. This allowed us to perform averaging in the universal timescale while keeping the Green's functions close to the equal time diagonal that account for the non-universal timescale. Mathematical details of our numerical implementation are explained in the appendix.

For all systems, the Kondo temperature of the dot is much smaller than the system temperature when the coupling of the dot to the leads is Γ_1 , therefore, the Kondo resonance does not exist in this state for all practical purposes. The spectral function consists of the broad virtual level of width $\sim 2\Gamma_1$ centered roughly at ϵ_{dot} . When the

coupling is abruptly switched, a new virtual-level resonance of width $\sim 2\Gamma_2$ is formed around the dot level in the non universal timescale. The time scale for the formation of this resonance is Γ_2 [17]. The Kondo resonance is formed in the universal timescale.

3. Non-universal timescale

First of all, we would like to make the distinction between changing the dot-lead tunneling constant and changing the dot level which was considered before[1]. In Fig. 1, we plot the instantaneous conductance for both cases for *system one* at a temperature well above T_K in infinitesimal bias to be able to make both the non-universal and universal timescales visible. We intentionally use slightly different ϵ_{dot}/Γ_1 in initial states for two cases to be able to shift the curves so that the difference would be visible. The final ϵ_{dot}/Γ_2 is the same for both cases therefore both curves gradually merge in the universal timescale. If we pick the same ϵ_{dot}/Γ_1 for both cases, the instantaneous conductances in the universal timescale perfectly overlap, thus the only difference between changing the dot-lead constant and changing the dot level lies in the non-universal timescale.

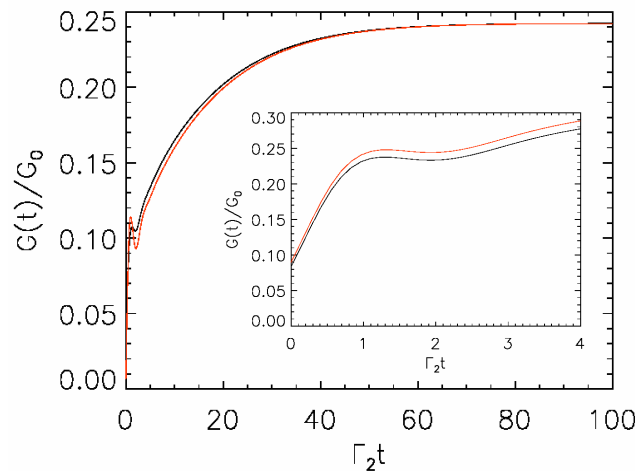


Figure 1. Comparison of instantaneous conductance for the cases of changing dot-lead coupling constant and the dot level. We show the rise of the conductance in the final state for *system one*. The calculation was carried out at $T=0.02\Gamma_2$ to make both timescales visible. The red curve corresponds to changing the dot level abruptly and the black curve is for changing the dot-lead tunneling constant. Both curves merge gradually in the universal timescale. In the inset, we show the rise of the conductance *system one* right after the coupling to the leads is switched. The black curve is for $T=0.005T_K$ and the red curve is for $T=0.003T_K$.

We start our analysis with the conductance results in the non-universal timescale. In the inset of Fig. 1, we display the rise of the instantaneous conductance for *system one* for two different temperatures right after the coupling of the dot to the leads is

switched to Γ_2 in infinitesimal bias. It is quite clear from these results that we have robust oscillations reminiscent of Rabi oscillations in this timescale regardless of the temperature. In order to understand the origin of these fast oscillations, we have to recall that the spin flips that give rise to the Kondo resonance are absent in this timescale and the only process that takes place is the charge relaxation. This implies that we can neglect the spin dependent terms in Eq. (1) and solve the remaining part. There are various ways of doing this. Here, we will follow the master equation approach[30]. In this approach, one can come up with an exact solution for $U=0$ in Eq. (1) in the wide band limit. The master equation is given by

$$\frac{dn(t)}{dt} + \Gamma(t)n(t) = -\sqrt{\Gamma(t)} \int_{t_0}^t d\bar{t} \sqrt{\Gamma(\bar{t})} \frac{\sin(\varepsilon_{dot}(t-\bar{t}))}{\beta \sinh(\frac{\pi(t-\bar{t})}{\beta})} e^{-\int_{\bar{t}}^t d\tau \frac{\Gamma(\tau)}{2}}, \quad (5)$$

where $\Gamma(t)$ is the linewidth of the Fano resonance in Eq. (2) and $n(t)$ is the instantaneous probability for finding an electron in the dot level,

$$n(t) = \sum_{\sigma} \langle \sigma | G^<(t, t) | \sigma \rangle, \quad (6)$$

where $|\sigma\rangle$ correspond to the spin up and down states of the dot level and $G^<(t, t)$ is the equal time component of the double time less than Green's function[30].

We will refer to $n(t)$ as the population from now on. In order to solve Eq. (5) for the case where we abruptly change the lifetime broadening of discrete state at $t = t_1$, we use

$$\Gamma(t) = \begin{cases} \Gamma_1 & \text{if } t_0 < t \leq t_1 \\ \Gamma_2 & \text{if } t > t_1 \end{cases}$$

together with the initial condition $n(t_0) = n_0$. Therefore, if $t > t_1$, Eq. (5) becomes

$$\begin{aligned} \frac{dn(t)}{dt} + \Gamma_2 n(t) &= -\sqrt{\Gamma_2} \int_{t_1}^t d\bar{t} \sqrt{\Gamma_2} \frac{\sin(\varepsilon_{dot}(t-\bar{t}))}{\beta \sinh(\frac{\pi(t-\bar{t})}{\beta})} e^{-\frac{\Gamma_2}{2}(t-\bar{t})} \\ &\quad - \sqrt{\Gamma_2} \int_{t_0}^{t_1} d\bar{t} \sqrt{\Gamma_1} \frac{\sin(\varepsilon_{dot}(t-\bar{t}))}{\beta \sinh(\frac{\pi(t-\bar{t})}{\beta})} e^{-\frac{\Gamma_2}{2}(t-t_1)-\frac{\Gamma_1}{2}(t_1-\bar{t})}. \end{aligned} \quad (7)$$

In Eq. (7), the second term on the right-hand side accounts for the evolution of the unperturbed system, hence we can discard its effect in the transient region. Since we are interested in the region where $t \gg t_1$, we can safely ignore the second exponential in the denominator in the first term on the right hand side as well. After these simplifications, Eq. (7) becomes

$$\begin{aligned} \frac{dn(t)}{dt} + \Gamma_2 n(t) &= -\sqrt{\Gamma_1 \Gamma_2} e^{-\frac{\Gamma_2}{2}(t-t_1)} \frac{2}{\beta} e^{-\frac{\Gamma_2}{2}t_1 - \frac{\pi}{\beta}t} \\ &\quad \left(\frac{e^{(\frac{\Gamma_1}{2} + \frac{\pi}{\beta})t_1} (\varepsilon_{dot} \cos(\varepsilon_{dot}(t-t_1)) + (\frac{\Gamma_1}{2} + \frac{\pi}{\beta}) \sin(\varepsilon_{dot}(t-t_1)))}{(\frac{\Gamma_1}{2} + \frac{\pi}{\beta})^2 + \varepsilon_{dot}^2} - \right. \\ &\quad \left. \frac{e^{(\frac{\Gamma_1}{2} + \frac{\pi}{\beta})t_0} (\varepsilon_{dot} \cos(\varepsilon_{dot}(t-t_0)) + (\frac{\Gamma_1}{2} + \frac{\pi}{\beta}) \sin(\varepsilon_{dot}(t-t_0)))}{(\frac{\Gamma_1}{2} + \frac{\pi}{\beta})^2 + \varepsilon_{dot}^2} \right). \end{aligned} \quad (8)$$

This is a nonhomogeneous first-order differential equation and it can be solved in a straightforward way. Time evolution of $n(t)$ in the second region becomes

$$\begin{aligned}
n(t) = & -a\varepsilon_{dot}e^{(-\frac{\Gamma_2}{2}-\frac{\pi}{\beta})t} \frac{\cos(\varepsilon_{dot}(t-t_1) - \arctan(\frac{\varepsilon_{dot}}{(\frac{\Gamma_2}{2}-\frac{\pi}{\beta})}))}{\sqrt{(\frac{\Gamma_2}{2}-\frac{\pi}{\beta})^2 + \varepsilon_{dot}^2}} \\
& - a(\frac{\Gamma_1}{2} + \frac{\pi}{\beta})e^{(-\frac{\Gamma_2}{2}-\frac{\pi}{\beta})t} \frac{\cos(\varepsilon_{dot}(t-t_1) - \pi - \arctan(\frac{(\frac{\Gamma_2}{2}-\frac{\pi}{\beta})}{-\varepsilon_{dot}})))}{\sqrt{(\frac{\Gamma_2}{2}-\frac{\pi}{\beta})^2 + \varepsilon_{dot}^2}} \\
& b\varepsilon_{dot}e^{(-\frac{\Gamma_2}{2}-\frac{\pi}{\beta})t} \frac{\cos(\varepsilon_{dot}(t-t_0) - \arctan(\frac{\varepsilon_{dot}}{(\frac{\Gamma_2}{2}-\frac{\pi}{\beta})}))}{\sqrt{(\frac{\Gamma_2}{2}-\frac{\pi}{\beta})^2 + \varepsilon_{dot}^2}} \\
& b(\frac{\Gamma_1}{2} + \frac{\pi}{\beta})e^{(-\frac{\Gamma_2}{2}-\frac{\pi}{\beta})t} \frac{\cos(\varepsilon_{dot}(t-t_0) - \pi - \arctan(\frac{(\frac{\Gamma_2}{2}-\frac{\pi}{\beta})}{-\varepsilon_{dot}})))}{\sqrt{(\frac{\Gamma_2}{2}-\frac{\pi}{\beta})^2 + \varepsilon_{dot}^2}}
\end{aligned} \tag{9}$$

where

$$a = \frac{2\sqrt{\Gamma_1\Gamma_2}e^{(\frac{\Gamma_2}{2}+\frac{\pi}{\beta})t_1}}{\beta(\frac{\Gamma_1}{2}+\frac{\pi}{\beta})^2 + \beta\varepsilon_{dot}^2} \tag{10}$$

and

$$b = \frac{2\sqrt{\Gamma_1\Gamma_2}e^{(\frac{\Gamma_1}{2}+\frac{\pi}{\beta})t_0}e^{\frac{\Gamma_2-\Gamma_1}{2}t_1}}{\beta(\frac{\Gamma_1}{2}+\frac{\pi}{\beta})^2 + \beta\varepsilon_{dot}^2}. \tag{11}$$

In Fig. 2, we display the numerically obtained population immediately after the dot-lead tunneling constant was switched to its final value together with the analytical solution obtained above for the spinless Anderson Hamiltonian. The same parameters were used for both cases. We first compare the results for *system one* and another configuration whose dot level and coupling constants are exactly half of *system one*, thus $\varepsilon_{dot}/\Gamma_1$ and $\varepsilon_{dot}/\Gamma_2$ are the same for both. It is obvious from Fig. 2 that the oscillation frequency of *system one* is twice as much as the new configuration in both analytical and numerical solutions. The oscillation frequency of the numerical and analytical solutions are the same as well. We reduced Γ_2 of the new configuration such that $\Gamma_2=2\Gamma_1$ to test the amplitudes and this reduces the amplitude of the oscillations keeping the frequency constant in both numerical and analytical solutions. Therefore, the qualitative analytical solution mimics the behaviour of the numerical population remarkably well even though the actual numerical values differ slightly due to the simplicity of the analytical approach.

Since the instantaneous conductance is related to the population by

$$G(t) \propto \frac{dn(t)}{dt}, \tag{12}$$

we reach the conclusion that the instantaneous conductance in the non-universal timescale is governed by the spinless Anderson Hamiltonian and that the instantaneous conductance oscillates sinusoidally with a frequency equal to the dot level as it can be seen from Eq. (9). The magnitude of the oscillations have more complicated form and they depend on Γ_1 , Γ_2 and ε_{dot} as Eq. (10) and (11) show.

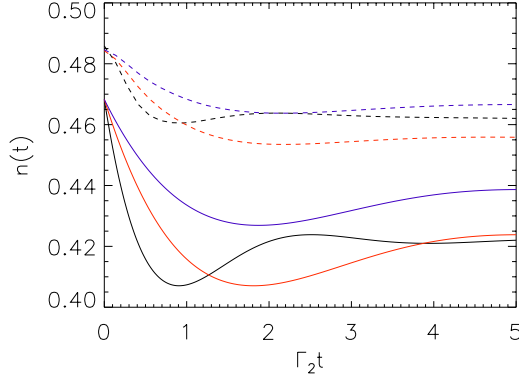


Figure 2. Evolution of the population in the non-universal timescale. Dashed curves show the numerical data right after the dot-lead tunneling constant is switched to its final value at $T=0.005\Gamma_2$ and solid curves are the result of the analytic solution of the spinless Anderson Hamiltonian for the same parameters. The black curves correspond to *system one*. ϵ_{dot} , Γ_1 and Γ_2 are half of *system one* for red curves. ϵ_{dot} and Γ_1 are half of *system one* and $\Gamma_2=2\Gamma_1$ for blue curves.

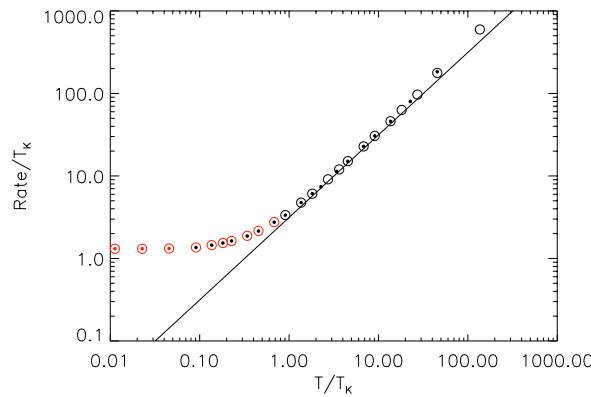


Figure 3. Rise rate, which is defined as the time it takes for instantaneous conductance to reach its final value, for *system one* and *system two* versus temperature T in infinitesimal bias. The solid dots are for *system one* and open circles are for *system two*. Black circles and dots represent the data obtained previously [1]. Red circles and dots correspond to the data taken with the new numerical scheme. The straight line has a slope of π and passes through the origin.

4. Universal timescale

Even though universal scaling behaviour was demonstrated in steady state nonequilibrium by using the perturbative renormalization group [28], it is not obvious

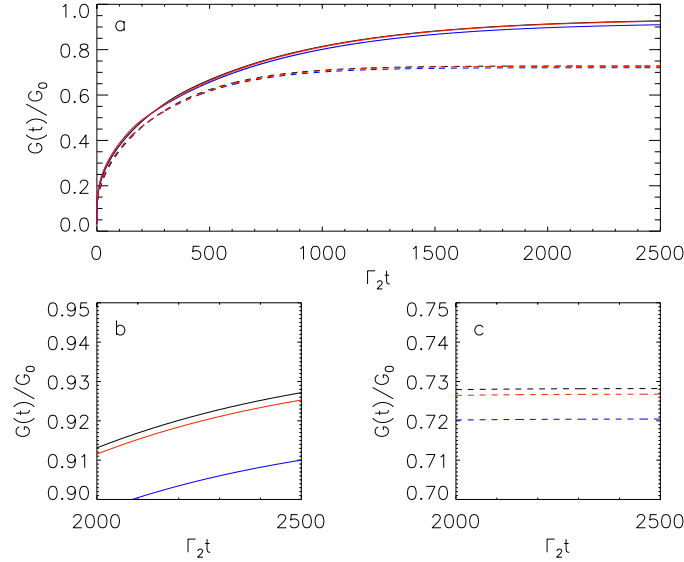


Figure 4. Convergence of time-dependent conductance curves for *system two*. Solid curves in panel a correspond to $T=0.0005\Gamma_2$, whereas dashed curves are for $T=0.0015\Gamma_2$. Black, red and blue curves correspond to grid sizes of 20, 40 and 80 respectively. Panels b and c magnify the long time part of panel a.

that the same arguments can be extended to a time dependent situation. A preliminary investigation has been carried out previously [1] for the latter and it turns out that the universality arguments seem to hold for time dependent situation as well even though these calculations have been done at temperatures around and above T_K .

In this work, we want to investigate this thoroughly at temperatures well below T_K . We are now in the Kondo timescale where spin relaxation takes place and it is governed by the full Anderson Hamiltonian therefore there is no closed form solution here due to strong correlations unlike the situation for the non-universal timescale. In order to demonstrate the universal scaling behaviour in this regime we use systems with different T_K and compare the resulting instantaneous conductance curves. One slight complication is that we have to rescale the results for different systems since the rise time, which is defined as the time to reach the steady state value in the final state, is different for each system therefore we have to find the correct scaling factor. We show the rise rates extracted from *system one* and *system two* in Fig. 3. The new numerical scheme allows us to go down to a fraction of T_K which was previously unavailable. The procedure we follow to extract these rates is identical to the one used previously[1] and we combined the results obtained there with our results for the sake of consistency. It is clear from these results that the rise rate of *system two* is almost twice as much as *system one*. This suggests that rise rate scales with T_K in general. Another important conclusion is that the rise rate saturates around $1.3T_K$ after T/T_K gets smaller than approximately 0.1. This is very close to the theoretically predicted Korringa rate.

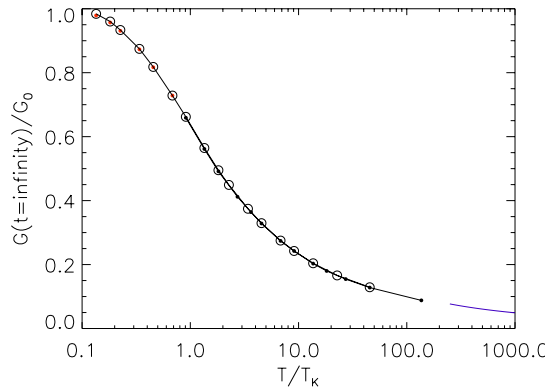


Figure 5. The large time limit of $G(t)/G_0$ vs. temperature for *system one* and *system two*. These are the final steady state conductance values in infinitesimal bias. Open circles correspond to *system one* and solid dots are for *system two*. Black circles and dots correspond to the data obtained previously [1] and red dots represent the data taken with the new numerical scheme. The blue line is the large T asymptote.

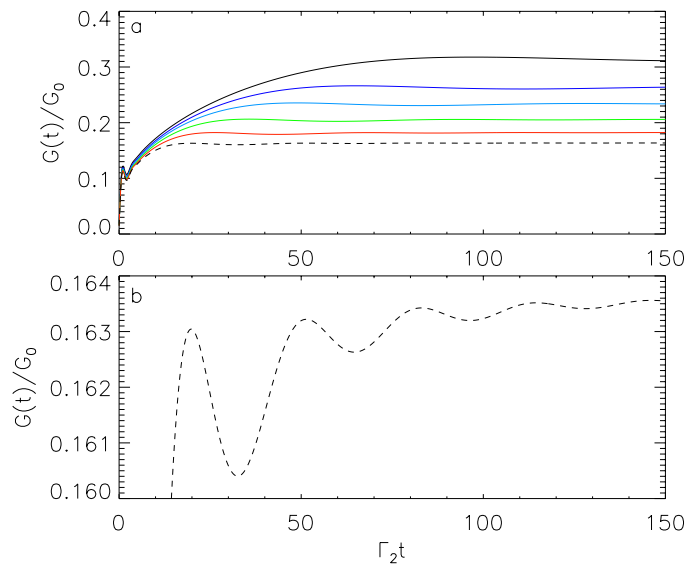


Figure 6. Rise of the instantaneous conductance in the universal timescale in finite bias for *system one* at $T=0.17T_K$ right after the coupling to the leads is switched. Black, dark blue, light blue, green, red and dashed black curves correspond to $V=0.04\Gamma_2$, $0.06\Gamma_2$, $0.08\Gamma_2$, $0.11\Gamma_2$, $0.15\Gamma_2$, $0.2\Gamma_2$ respectively in panel a. In panel b, we show the instantaneous conductance for $V=0.2\Gamma_2$ in magnified scale.

In Fig. 4 we demonstrate the convergence of the conductance curves for *system two* for two different temperatures right after the dot-lead tunneling constant is switched to

its final value. In order to do so, we plotted the instantaneous conductance curves for different grid sizes, which is defined as the number of elements in the fine grid over which the averaging takes place as explained in the appendix, while keeping all other numerical parameters constant. As we see in the magnified panels, we achieve good convergence as we reduce the grid size. We also would like to point out that a comparison of the x axis values for Fig. 4 and the inset of Fig. 1 reveals quite clearly that the universal timescale is much longer than non-universal timescale.

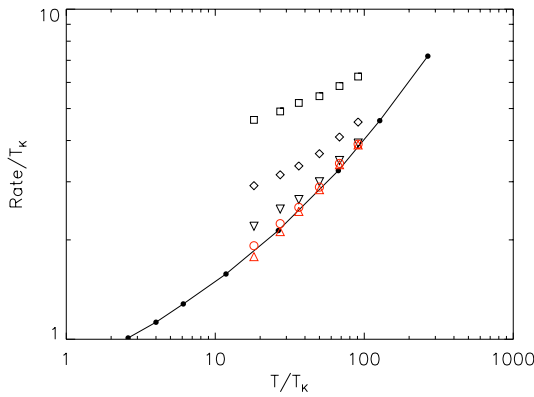


Figure 7. Decay of SKP oscillations vs. bias V for *system one*. Solid circles represent the analytical calculations of 1.8γ at zero temperature [28]. Black squares, diamonds and downwards triangles are previous results[1] and correspond to $T=1.4T_K$, $0.69T_K$ and $0.34T_K$ respectively. Red open circles and upwards triangles are for $T=0.17T_K$ and $0.08T_K$.

In Fig. 5, we plot the final steady state conductances obtained from the converged curves in Fig. 4 alongside with the exact asymptotic curve at large $\ln(T/T_K)$ which is given by

$$\frac{G}{G_0} = \frac{3\pi^2}{16 \ln^2(T/T_K)}, \quad (13)$$

which was first calculated by Abrikosov[1] and later adapted to quantum dots[33]. We again plotted the results obtained previously[1] together with the results taken with the new numerical scheme. The new scheme allows us to handle temperatures well below T_K for T_K as low as 1 K. The results in Fig. 5 clearly demonstrate that the universality is preserved for temperatures down to a fraction of T_K . Our conductance results for temperatures lower than $T/T_K=0.1$ in Fig. 4 exceed the unitarity limit thus they are not shown. This is a well known pathology of NCA and it was pointed out before[28].

We believe the tiny deviations observed in the final steady state would disappear if we could study a system for which the Fano resonance has negligible overlap with the Fermi level. This is presently out of our reach. This is mainly due to the fact that the rise time scales with T_K as we demonstrated above. We need to study a system which

has T_K around a few nanokelvin to make the overlap of the Fano resonance with the Fermi level less than one percent since the broadening has a lorentzian lineshape. This is computationally not feasible at the moment.

We finally would like to investigate the instantaneous conductance at large bias. When we apply finite bias to the system, Kondo resonances that form at each lead's Fermi level split. Due to the finite bias, these resonances are broadened compared to the infinitesimal bias situation[26]. It has recently been established that the quantum beating between these split Kondo peaks gives rise to sinusoidal oscillations in the instantaneous conductance after it reaches its final state[26, 31] and the frequency of these oscillations is equal to the magnitude of the bias[1].

In this work, we investigate these SKP oscillations down to zero temperature. In Fig. 6, we display the instantaneous conductance right after the tunneling constant is switched to its final state for a variety of biases at constant temperature. As the bias increases, so does the frequency of the SKP oscillations, however, the final steady state value of the conductance goes down. This is due to the fact that decoherence destroys the Kondo effect. We also show the instantaneous conductance for the largest bias in a magnified scale. Damped sinusoidal oscillations are visible clearly here.

It is intriguing to investigate to what extent the damping rate of these oscillations changes as we change temperature. We follow the same procedure used previously[1] to determine the damping rate. We plot the difference between the final steady state value of the conductance and the values at each minima in a logarithmic scale and the slope of the linear best fit curve gives the decay rate. We display half the decay rates we determined together with the previously obtained values[1] in Fig. 6. It is obvious that the decay rates of SKP oscillations saturate as we approach zero temperature. We also show the zero temperature analytical results[28] in the same figure. We find that half the decay rates we determine from our NCA calculations correspond to roughly 1.8 times the decoherence rate obtained from perturbative renormalization group. The latter calculations do not correspond to physical observables, therefore, there does not need to be a one to one correspondence between the two cases, nevertheless, it would be interesting to see what the outcome of an experiment would show.

5. Conclusion

In this paper, we analyzed the transient conductance in the non-universal and universal timescales for single electron transistor when the dot-lead tunneling constant is suddenly switched to a value where the Kondo effect is present. In the non-universal timescale, we saw sinusoidal oscillations and we explained them qualitatively with the solution of the spinless Anderson Hamiltonian. In the universal timescale, we computed the conductance for two systems with different Kondo temperatures in infinitesimal bias and compared the results down to a fraction of T_K . Our results show that the universality arguments put forward for steady-state transport previously hold for time dependent situations as well in spite of tiny deviations.

We also determined the decay rates of recently identified SKP oscillations down to zero temperature and compared our NCA results with the analytical decoherence rates obtained from the perturbative renormalization group. We found that half of the decay rates we obtained from NCA roughly correspond to 1.8 times decoherence rate obtained from the perturbative renormalization group. We hope that these predictions motivate future experiments.

We thank National Center for Supercomputer Applications for supercomputer time. This work was supported by the Welch Foundation at Rice. Upon completion of this manuscript, we became aware of another work[34] in which an analytical result based on resonant-level model was obtained for the non-universal timescale.

- [1] Plihal M, Langreth D C and Nordlander P 2005 *Phys. Rev. B* **71** 165321
- [2] Anders F B and Schiller A 2005 *Phys. Rev. Lett.* **95** 196801
- [3] Elzerman J M, Hanson R, Willems van Beveren L H, Witkamp B, Vandersypen L M K and Kouwenhoven L P 2004 *Nature(London)* **430** 431
- [4] Kondo J 1964 *Prog. Theor. Phys.* **32** 37
- [5] Kouwenhoven L P and Glazman L I 2001 *Phys. World* **14** 33
- [6] Merino J and Marston J B 2004 *Phys. Rev. B* **69** 115304
- [7] Ng T K and Lee P A 1988 *Phys. Rev. Lett.* **61** 1768
- [8] Glazman L I and Raikh M E 1988 *JETP Lett.* **47** 452
- [9] Hershfield S, Davis J H and Wilkins J W 1991 *Phys. Rev. Lett.* **67** 3720
- [10] Goldhaber-Gordon D, Shtrikman H, Mahalu D, Abusch-Magder D, Meirav U and Kastner M A 1998 *Nature(London)* **391** 156
- [11] Goldhaber-Gordon D, Gores J, Kastner M A, Shtrikman H, Mahalu D and Meirav U 1998 *Phys. Rev. Lett.* **81** 5225
- [12] Cronenwett S M, Osterkamp T H and Kouwenhoven L P 1998 *Science* **281** 540
- [13] Hettler M H and Schoeller H 1995 *Phys. Rev. Lett.* **74** 4907
- [14] Schiller A and Hershfield S 1996 *Phys. Rev. Lett.* **77** 1821
- [15] Ng T K 1996 *Phys. Rev. Lett.* **76** 487
- [16] Lobaskin D and Kehrein S 2005 *Phys. Rev. B* **71** 193303
- [17] Nordlander P, Pustilnik M, Meir Y, Wingreen N S and Langreth D C 1999 *Phys. Rev. Lett.* **83** 808
- [18] Goldin Y and Avishai Y 1998 *Phys. Rev. Lett.* **81** 5394
- [19] Kaminski A, Nazarov Y V and Glazman L I 1999 *Phys. Rev. Lett.* **83** 384
- [20] Kogan A, Amasha S and Kastner M A 2004 *Science* **304** 1293
- [21] Aguado R and Langreth D C 2000 *Phys. Rev. Lett.* **85** 1946; 2003 *Phys. Rev. B* **67** 245307
- [22] Jeong H, Chang A M and Melloch M R 2001 *Science* **293** 2221
- [23] Craig N J, Taylor J M, Lester E A, Marcus C M, Hanson M P and Gossard A C 2004 *Science* **304** 565
- [24] Plihal M, Langreth D C and Nordlander P 2000 *Phys. Rev. B* **61** R13341
- [25] Schiller A and Hershfield S 2000 *Phys. Rev. B* **62** R16271
- [26] Wingreen N S and Meir Y 1994 *Phys. Rev. B* **49** 11040
- [27] Bickers N E 1987 *Rev. Mod. Phys.* **59** 845
- [28] Rosch A, Kroha J and Wölfle P 2001 *Phys. Rev. Lett.* **87** 156802
- [29] Shao H, Langreth D C and Nordlander P 1994 *Phys. Rev. B* **49** 13929
- [30] Langreth D C and Nordlander P 1991 *Phys. Rev. B* **43** 2541
- [31] Sivan N and Wingreen N S 1996 *Phys. Rev. B* **54** 11622
- [32] Abrikosov A A 1965 *Physics(N.Y.)* **2** 5
- [33] Nordlander P, Wingreen N S, Meir Y and Langreth D C 2001 *Phys. Rev. B* **61** 2146
- [34] Anders F B and Schiller A 2006 *cond-mat/0604517*

Appendix A. Details of the numerical implementation

In this appendix, the Dyson equations are discretized and the method of solution is presented. We start with retarded Green's functions. The Dyson equations for $g_\sigma(t, t')$ and $b(t, t')$ for $t \geq t'$ are

$$\frac{\partial}{\partial t} g_\sigma(t, t') = - \int_{t'}^t d\bar{t} \tilde{K}_\sigma^>(t, \bar{t}) b(t, \bar{t}) g_\sigma(\bar{t}, t'), \quad (\text{A.1})$$

$$\frac{\partial}{\partial t} b(t, t') = - \sum_\sigma \int_{t'}^t d\bar{t} \tilde{K}_\sigma^<(\bar{t}, t) g_\sigma(t, \bar{t}) b(\bar{t}, t'). \quad (\text{A.2})$$

For $t < t'$ the $g_\sigma(t, t')$ and $b(t, t')$ functions can be determined by

$$\begin{aligned} g_\sigma(t', t) &= g_\sigma^*(t, t'), \\ b(t', t) &= b^*(t, t'). \end{aligned} \quad (\text{A.3})$$

We can represent the Green's functions as

$$\begin{aligned} g_\sigma(t, t') &= g_\sigma^f(t, t') e^{i\omega_g(t-t')}, \\ b(t, t') &= b^f(t, t') e^{i\omega_b(t-t')}, \end{aligned} \quad (\text{A.4})$$

where $e^{i\omega_g(t-t')}$ and $e^{i\omega_b(t-t')}$ are the oscillatory ‘‘carrier’’ parts and $g_\sigma^f(t, t')$ and $b^f(t, t')$ denote smooth, envelope-like modulating functions. By substituting Eqs. (A.4) in Eqs. (A.1) and (A.2) one can obtain

$$\begin{aligned} \frac{\partial}{\partial t} [g_\sigma^f(t, t') e^{i\omega_g(t-t')}] &= - \int_{t'}^t d\bar{t} \tilde{K}^>(\bar{t}, t) e^{i\omega_b(\bar{t}-t)} e^{i\omega_g(\bar{t}-t')} \\ &\quad b^f(\bar{t}, t) g_\sigma^f(\bar{t}, t'), \end{aligned} \quad (\text{A.5})$$

$$\begin{aligned} \frac{\partial}{\partial t} [b^f(t, t') e^{i\omega_b(t-t')}] &= - \sum_\sigma \int_{t'}^t d\bar{t} \tilde{K}^<(\bar{t}, t) e^{i\omega_g(\bar{t}-t)} e^{i\omega_b(\bar{t}-t')} \\ &\quad g_\sigma^f(\bar{t}, t) b^f(\bar{t}, t'). \end{aligned} \quad (\text{A.6})$$

In steady state, both kernels depend only on the time difference rather than on individual values of t and \bar{t} . The kernels can be combined with the oscillatory parts in the following manner

$$\begin{aligned} \tilde{K}_\sigma^>(t, \bar{t}) e^{i\omega_b(t-\bar{t})} e^{i\omega_g(\bar{t}-t')} &= \tilde{K}_\sigma^>(t, \bar{t}) e^{i(\omega_b-\omega_g)(t-\bar{t})} e^{i\omega_g(t-t')} \\ &= \tilde{K}_{\sigma\omega}^>(t-\bar{t}) e^{i\omega_g(t-t')}, \end{aligned} \quad (\text{A.7})$$

and

$$\begin{aligned} \tilde{K}_\sigma^<(\bar{t}, t) e^{i\omega_g(t-\bar{t})} e^{i\omega_b(\bar{t}-t')} &= \tilde{K}_\sigma^<(\bar{t}, t) e^{i(\omega_g-\omega_b)(t-\bar{t})} e^{i\omega_b(t-t')} \\ &= \tilde{K}_{\sigma\omega}^<(\bar{t}-t) e^{i\omega_b(t-t')}. \end{aligned} \quad (\text{A.8})$$

Let us illustrate our discretization scheme on the following integral

$$\int_{t'}^t d\bar{t} \tilde{K}_{\sigma\omega}^<(\bar{t}, t) g_\sigma^f(\bar{t}, t) b^f(\bar{t}, t') = \sum_i \int_{\Delta_i} d\bar{t} \tilde{K}_{\sigma\omega}^<(\bar{t}, t) g_\sigma^f(\bar{t}, t) b^f(\bar{t}, t') \quad (\text{A.9})$$

$$= \sum_i g_\sigma^f(t, \bar{\xi}_i) b^f(\bar{\xi}_i, t') \int_{\Delta_i} d\bar{t} \tilde{K}_{\sigma\omega}^<(\bar{t}, t), \quad (\text{A.10})$$

where $\Delta_i = [\bar{t}_i, \bar{t}_{i+1}]$ is the i -th coarse grid interval and $\bar{\xi}_i \in \Delta_i$. Also we assume that

$$g_\sigma^f(t, \bar{\xi}_i) b^f(\bar{\xi}_i, t') \cong \frac{1}{2} [g_\sigma^f(t, \bar{t}_i) b^f(\bar{t}_i, t') + g_\sigma^f(t, \bar{t}_{i+1}) b^f(\bar{t}_{i+1}, t')]. \quad (\text{A.11})$$

This approximation is valid because the g_σ^f and b^f functions behave almost linearly. To obtain accurate estimate for the oscillatory kernel integration in Eq. (A.10) we use a finer grid with spacing δ and Simpson's quadrature

$$\int_{\Delta_i} \tilde{K}_{\sigma\omega}^>(t, \bar{t}) d\bar{t} \cong \sum_j w_j \tilde{K}_{\sigma\omega}^>(t - \bar{t}_j) = \tilde{K}_{\sigma P}^>(t, \bar{t}_i), \quad (\text{A.12})$$

and

$$\int_{\Delta_i} \tilde{K}_{\sigma\omega}^<(\bar{t}, t) d\bar{t} \cong \sum_j w_j \tilde{K}_{\sigma\omega}^<(\bar{t}_j - t) = \tilde{K}_{\sigma P}^<(\bar{t}_i, t), \quad (\text{A.13})$$

where w_j are the weights. Due to the kernels translational invariancy one can precompute $\tilde{K}_{\sigma P}^>(t, \bar{t}_i)$ and $\tilde{K}_{\sigma P}^<(\bar{t}_i, t)$ values and keep them in the core memory during calculation. In the differential part we use the finite difference method only for the non-periodic part

$$\begin{aligned} \frac{\partial}{\partial t} \left[g_\sigma^f(t, t') e^{i\omega_g(t-t')} \right] &\cong e^{i\omega_g(t-t')} \\ &\left[i\omega_g g_\sigma^f(t, t') + \frac{g_\sigma^f(t, t') - g_\sigma^f(t - \Delta, t')}{\Delta} \right]. \end{aligned} \quad (\text{A.14})$$

The discretized version of Eqs. (A.5) and (A.6) can be written as

$$\begin{aligned} \left(1 + \frac{i\Delta\omega_g}{2}\right) g_\sigma^f(m, n) &= \left(1 - \frac{i\Delta\omega_g}{2}\right) g_\sigma^f(m-1, n) \\ &- \frac{1}{2}\Delta^2 \sum_{j=n}^m c_j \tilde{K}_{\sigma P}^>(m, j) b^f(m, j) g_\sigma^f(j, n) \\ &- \frac{1}{2}\Delta^2 e^{-i\Delta\omega_g} \sum_{j=n}^{m-1} c_j \tilde{K}_{\sigma P}^>(m-1, j) b^f(m-1, j) g_\sigma^f(j, n) \end{aligned} \quad (\text{A.15})$$

and

$$\begin{aligned} \left(1 + \frac{i\Delta\omega_b}{2}\right) b^f(m, n) &= \left(1 - \frac{i\Delta\omega_b}{2}\right) b^f(m-1, n) \\ &- \frac{1}{2}\Delta^2 \sum_{\sigma} \sum_{j=n}^m c_j \tilde{K}_P^<(j, m) g_\sigma^f(m, j) b^f(j, n) \\ &- \frac{1}{2}\Delta^2 e^{-i\Delta\omega_b} \sum_{\sigma} \sum_{j=n}^{m-1} c_j \tilde{K}_P^<(j, m-1) g_\sigma^f(m-1, j) b^f(j, n) \end{aligned} \quad (\text{A.16})$$

where we use integers i , j , m , and n for the time arguments, with consecutive integers representing a time difference of Δ , the coarse grid spacing. In Eqs. (A.15) and (A.16) $c_j = 1/2$ for $j = n$, m or $m-1$ and it equals unity in all other cases. These equations have the same algebraic structure as reported before (see Shao *et al.*). The computational scaling of the equations solving is N^3 , where N is the number of coarse mesh grid points. Therefore, it is crucial for the performance to reduce N as much as possible without losing accuracy appreciably. For that we formulate Dyson's equations with respect to the almost linearly behaving functions $g_\sigma^f(t, t')$ and $b^f(t, t')$. It allows us to use the coarse grid for discretized equations and fine grid δ for the kernels preintegration. To find good estimates for the frequencies ω_g and ω_b we use the previous implementation[29]

with coarse grid discretization and then extract frequencies from the Green's functions. We found that values of ω_g and ω_b are not sensitive to the quality of discretization and even the coarse grid is accurate for the frequency estimation.

The same preintegration scheme is valid for the "less than" Green's functions, therefore we present only the final discretized equations for them. In the $t \neq t'$ case we have the following system of equations

$$\begin{aligned} & \left(1 + \frac{i\Delta\omega_g}{2}\right) G_\sigma^<(m, n) + \frac{\Delta^2}{2} c_m \tilde{K}_{\sigma P}^>(m, m) G_\sigma^<(m, n) - \\ & \frac{\Delta^2}{2} c_n \tilde{K}_{\sigma P}^<(m, n) B^<(m, n) = G_\sigma(m, n) + \\ & \frac{\Delta^2}{2} c_n \tilde{K}_{\sigma P}^<(m-1, n) B^<(m-1, n) + \left(1 - \frac{i\Delta\omega_g}{2}\right) G_\sigma^<(m-1, n), \end{aligned} \quad (\text{A.17})$$

$$\begin{aligned} & \left(1 + \frac{i\Delta\omega_b}{2} + \frac{\Delta^2}{2} c_m \tilde{K}_{\sigma P}^<(m, n)\right) B^<(m, n) - \\ & \sum_\sigma \frac{\Delta^2}{2} c_n \tilde{K}_{\sigma P}^>(n, m) G_\sigma^<(m, n) = \sum_\sigma B_\sigma(m, n) + \\ & \sum_\sigma \frac{\Delta^2}{2} c_n \tilde{K}_{\sigma P}^>(n, m-1) G_\sigma^<(m-1, n) + \left(1 - \frac{i\Delta\omega_g}{2}\right) B^<(m-1, n), \end{aligned} \quad (\text{A.18})$$

where

$$\begin{aligned} G_\sigma(m, n) &= -\frac{\Delta^2}{4} c_{m-1} \tilde{K}_{\sigma P}^>(m-1, m-1) G_\sigma^<(m-1, n) + \\ & \frac{\Delta^2}{2} \sum_{i=m-1}^m \sum_{j=1}^{n-1} c_j \tilde{K}_{\sigma P}^<(i, j) B^<(i, j) g_\sigma^f(n, j)^* - \\ & \frac{\Delta^2}{2} \sum_{i=m-1}^m \sum_{j=1}^{i-1} c_j \tilde{K}_{\sigma P}^>(i, j) b^f(i, j) G_\sigma^<(j, n), \\ B_\sigma(m, n) &= -\frac{\Delta^2}{4} \tilde{K}_{\sigma P}^<(m-1, m-1) B^<(m-1, n) + \\ & \frac{\Delta^2}{2} \sum_{i=m-1}^m \sum_{j=1}^{n-1} c_j \tilde{K}_{\sigma P}^>(i, j) G_\sigma^<(i, j) b^*(n, j) - \\ & \frac{\Delta^2}{2} \sum_{i=m-1}^m \sum_{j=1}^{i-1} c_j \tilde{K}_{\sigma P}^<(j, i) g_\sigma^f(i, j) B^<(j, n). \end{aligned} \quad (\text{A.19})$$

For the $t = t'$ case

$$\begin{aligned} & G_\sigma^<(m, m) + \text{Re} \left(\frac{\Delta^2}{2} \tilde{K}_{\sigma P}^>(m, m) G_\sigma^<(m, m) \right) - \\ & \text{Re} \left(\frac{\Delta^2}{2} \tilde{K}_{\sigma P}^<(m, m) B^<(m, m) \right) = G_\sigma^<(m-1, m-1) + \\ & \text{Re} \left(\frac{\Delta^2}{2} \tilde{K}_{\sigma P}^<(m-1, m-1) B^<(m-1, m-1) \right) - \\ & \text{Re} \left(\frac{\Delta^2}{2} \tilde{K}_{\sigma P}^>(m-1, m-1) G_\sigma^<(m-1, m-1) \right) + \text{Re}(G_\sigma(m, n)), \end{aligned} \quad (\text{A.20})$$

$$\begin{aligned}
& -\text{Re} \left(\sum_{\sigma} \frac{\Delta^2}{2} \tilde{K}_{\sigma P}^>(m, m) G_{\sigma}^<(m, m) + \frac{\Delta^2}{2} \tilde{K}_{\sigma P}^<(m, m) B^<(m, m) \right) + \\
& B^<(m, m) = -\text{Re} \left(\frac{\Delta^2}{2} \tilde{K}_{\sigma P}^<(m-1, m-1) B^<(m-1, m-1) \right) - \\
& \sum_{\sigma} \text{Re} \left(-\frac{\Delta^2}{2} \tilde{K}_{\sigma P}^>(m-1, m-1) G_{\sigma}^<(m-1, m-1) + G_{\sigma}(m, n) \right) + \\
& B^<(m-1, m-1),
\end{aligned} \tag{A.21}$$

where

$$\begin{aligned}
G_{\sigma}(m, n) = & \Delta^2 \sum_{i=m-1}^m \sum_{j=1}^{i-1} c_j \tilde{K}_{\sigma P}^<(j, i) B^<(j, i) g_{\sigma}^f(i, j) - \\
& \Delta^2 \sum_{i=m-1}^m c_j \tilde{K}_{\sigma P}^>(i, j) b^f(i, j) G_{\sigma}^<(j, i).
\end{aligned} \tag{A.22}$$

As in the case of retarded Green's functions, these systems of linear equations can be treated by methods developed by Shao *et al*[29].

If we want to take into account the abrupt change of the dot-lead tunneling constant or the position of the dot level, we need to modify Eqs. (A.4) as

$$\begin{aligned}
g_{\sigma}(t, t') &= g_{\sigma}^f(t, t') e^{i\omega_{1g}(t-t')} + \theta(t-t_1) \theta(t'-t_1) \\
&\quad g_{\sigma}^f(t, t') (e^{i\omega_{2g}(t-t')} - e^{i\omega_{1g}(t-t')}), \\
b(t, t') &= b^f(t, t') e^{i\omega_{1b}(t-t')} + \theta(t-t_1) \theta(t'-t_1) \\
&\quad b^f(t, t') (e^{i\omega_{2b}(t-t')} - e^{i\omega_{1b}(t-t')}).
\end{aligned} \tag{A.23}$$

In Eqs. (A.23) ω_1 and ω_2 correspond to the oscillation frequencies of the first and second state respectively and t_1 is the time of the abrupt change. One can apply the two grids scheme for this case as well.